J. Fluid Mech. (2019), *vol.* 874, *pp.* 102–130.
doi:10.1017/jfm.2019.461

Mean velocity, spreading and entrainment characteristics of weak bubble plumes in unstratified and stationary water

Binbin Wang[1,†], **Chris C. K. Lai**[2] **and Scott A. Socolofsky**[3]

[1]Department of Civil and Environmental Engineering, University of Missouri, Columbia, MO 65211, USA

[2]Los Alamos National Laboratory, Los Alamos, NM 87545, USA

[3]Zachry Department of Civil Engineering, Texas A&M University, College Station, TX 77843, USA

(Received 15 July 2018; revised 3 June 2019; accepted 4 June 2019; first published online 3 July 2019)

In this paper we present an experimental and theoretical study of weak bubble plumes in unstratified and stationary water. We define a weak bubble plume as one that spreads slower than the linear rate of a classic plume. This work focuses on the characteristics of the mean flow in the plume, including centreline velocity, plume spreading and entrainment of ambient water. A new theory based on diffusive spreading instead of an entrainment hypothesis is used to describe the lateral spreading of the bubbles and the associated plume. The new theory is supported by the experimental data. With the measured data of liquid volume fluxes and the new theory, we conclude that the weak bubble plume is a decreasing entrainment process, with the entrainment coefficient α in the weak bubble plume decreasing with height z, following $\alpha \sim z^{-1/2}$, and taking on values much smaller than those in a classic bubble plume. An additional non-dimensional diffusion coefficient, $\hat{E}_t \sim E_t U_s^2/B_0$, is also needed to describe the evolution of the volume and kinematic momentum fluxes for the mean flow in the weak bubble plume. Here, E_t is the effective turbulent diffusion coefficient, U_s is the terminal rise velocity of the bubbles, and B_0 is the kinematic buoyancy flux of the source. Finally, we provide a unified framework for the mean flow characteristics, including volume flux, momentum flux and plume spreading for the classic and weak bubble plumes, which also provides insight on the transition from classic to weak bubble plume behaviour.

Key words: multiphase flow

1. Introduction

Multiphase plumes create important flow fields in a variety of natural and engineered fluid systems. In an unbounded domain, the drag force resulting from the relative movement of the buoyant dispersed-phase bubbles, drops or particles generates motion in the ambient continuous phase. For a point release in a stagnant ambient reservoir, the group effect of the dispersed phases may generate large-scale

† Email address for correspondence: wangbinb@missouri.edu

motion (i.e. larger than a particle wake) in the continuous phase, creating entrainment of ambient fluid due to velocity shear at the edge of the continuous-phase motion, and resulting in the development of a coherent plume of particles and continuous-phase fluid. Such multiphase plumes (referred to herein as classic multiphase plumes) include air bubble plumes for lake aeration (Wuest, Brooks & Imboden 1992) or for reservoir destratification (Asaeda & Imberger 1993; Lemckert & Imberger 1993; Schladow 1993), and subsea accidental oil and gas blowouts (Yapa & Zheng 1997; Zheng & Yapa 1998; Yapa, Zheng & Nakata 1999; Johansen 2000), among many others. In contrast, some multiphase releases are distributed or have relatively weak volume flow rate, yielding very low void fraction. As a result, the group effect of the dispersed phase and the turbulence of the continuous phase in the plume are weak, the ambient entrainment and transport are low, the mass and momentum carried in the plume are limited, and therefore a coherent plume may not form. In these cases, the plume spreading may be governed by different physics than in classic plumes. Here, we define such multiphase flows with low release rate and weak entrainment as weak multiphase plumes (Leitch & Baines 1989). One example of a weak bubble plume is natural gas seepage at low volume flux emanating from the ocean floor (Wang & Socolofsky 2015*b*; Wang *et al.* 2016). This paper uses laboratory experiments to quantify new aspects of the fundamental flow behaviour of weak bubble plumes, including the mean velocity, lateral spreading rate and entrainment process.

Understanding the physics of a weak bubble plume is important to predict the dynamics of natural gas seeps. Most of these seeps form weak bubble plumes due to the low flow rates of hydrocarbon bubbles that emanate from cracks on the seafloor. These plumes are ubiquitous on the continental margins and supply a considerable amount of methane to the methane budget in the oceans (Westbrook *et al.* 2009; Brothers *et al.* 2013; Talukder *et al.* 2013; Skarke *et al.* 2014; Weber *et al.* 2014; Johnson *et al.* 2015; Ruppel & Kessler 2017). Therefore, understanding weak bubble plumes helps to predict the characteristics of hydrocarbon bubbles in the oceans (e.g. bubble rise velocity) and the associated interaction between them and the ambient water (e.g. dissolution, transport). This information controls the lifetime of the dispersed phase and the vertical distribution of methane in the ocean water column.

Commonly, Lagrangian particle models are applied to predict the fate of individual natural gas bubbles during their ascent in the ocean, and the results of these models have been used to compare with the measured maximum height of rise of bubbles in flares observed above natural seeps (McGinnis *et al.* 2006; Romer *et al.* 2012). These models ignore entrainment and the vertical velocity of water in the plume and treat the bubble rise velocity as its terminal velocity in stationary water. Hence, an objective of this paper is to understand the velocity field of the continuous phase in a weak bubble plume and to assess the validity of the assumptions in present seep flare models.

One comprehensive investigation describing the behaviour of weak bubble plumes was carried out by Leitch & Baines (1989) – at gas flow rate at the source $Q_g(0) = 0.025$–0.375 NL min^{-1} (normal litres per minute) at standard temperature and pressure. They found that the weak bubble plume does not spread out linearly as in a classic plume, but rather follows the relationship $b_g \sim z^{1/2}$, where b_g is the Gaussian half-width of the plume and z is the vertical coordinate, positive upwards. Based on their experimental data, Leitch & Baines (1989) concluded that the entrainment process for classic plumes is not applicable in a weak bubble plume. However, their study only spanned a short range of height ($\leqslant 0.5$ m), which limits our ability to understand how weak bubble plumes evolve over large distances. In addition, an

explanation of the physical mechanism responsible for the square-root spreading rate of the weak bubble plume with height is still lacking. Moreover, the physics of plume spreading, entrainment and the velocity field in weak bubble plumes remains unclear.

In contrast to weak bubble plumes, classic bubble plumes have been extensively studied (Ditmars & Cederwall 1974; Milgram 1983; Asaeda & Imberger 1993; Socolofsky & Adams 2002, 2003, 2005; Crounse, Wannamaker & Adams 2007). The physics of entrainment is fundamental to the integral analysis of plumes, and was originally developed for single-phase buoyant plumes by Morton, Taylor & Turner (1956). A classic single-phase plume is self-similar, spreads linearly with height above the source (e.g. half-width $b_g \sim z$ for point source plumes), and turbulent entrainment determines the increase of the liquid volume flux $Q(z)$ in the plume, parametrized by an entrainment coefficient α and scaled with the plume centreline velocity U_c. Multiphase plumes are not strictly self-similar, exhibiting variable entrainment coefficients (Milgram 1983; Seol *et al.* 2007), but retain many features of an integral plume.

The main aspect of a multiphase plume that causes it to deviate from self-similarity is the relative velocity, or slip velocity, U_s of the dispersed phase. In a single-phase plume, the plume properties depend on the initial kinematic buoyancy flux $B_0 = gQ(0)(\rho_0 - \rho)/\overline{\rho}$ and the length scale z, the distance from the plume source. Here, g is the acceleration of gravity, ρ_0 is the average density of the discharged fluids (equal to the particle density ρ_p for a pure dispersed-phase plume), ρ is the density of the ambient fluid, and $\overline{\rho}$ is a characteristic density of the receiving reservoir (e.g. using the Boussinesq approximation in density stratification). In a multiphase plume, U_s and B_0 can be combined to form another length scale (e.g. B_0/U_s^3), and this second length scale breaks the requirements for self-similarity. This dispersed-phase length scale appears in various forms proposed in Mcdougall (1978), Schladow (1992) and Asaeda & Imberger (1993). Bombardelli (2004) proposed the length scale D, which has subsequently been used in other studies (Garcia & Garcia 2006; Bombardelli *et al.* 2007), given as

$$D = \frac{B_0}{4\pi\alpha^2 U_s^3}, \tag{1.1}$$

where $\alpha = 0.083$ is the pure plume entrainment coefficient. Bombardelli *et al.* (2007) use an integral model to show that all multiphase plumes reach an asymptotic state (i.e. they forget their initial geometry) for $z/D > 5$, where the normalized velocity of the continuous-phase mean flow collapses onto a universal curve. However, there is little experimental data within this asymptotic regime. In addition, it is not known whether this asymptotic solution for the mean velocity would still hold when z/D approaches values that are orders of magnitude higher than 5, as occurs in natural seeps in the oceans.

The above observations lead to a key question: Does the bubble plume act as a coherent plume when $z/D \gg 5$, or in general when $z/D \gg O(1)$? Two scenarios can lead to large z/D: (1) a bubble plume rising in an infinite vertical environment, i.e. $z \to \infty$; and (2) a bubble plume having a very small gas flow rate, i.e. $B_0 \to 0$. In the first scenario, when a bubble plume rises towards large z/D, the void fraction decreases and becomes very small as the plume spreads out. Eventually, bubbles become independent of any group effects and the bubble plume may no longer behave as a classic plume. In the second scenario, the initial void fraction is very low due to low $Q_g(0)$, and the plume may not behave as a classic plume even close to the bubble source. To maximize z/D in this study, we design a set of experiments

to investigate the weak bubble plume with two different small flow rates (giving small B_0) in a very deep laboratory tank (giving large z).

The focus of this paper is to quantify the characteristics of the mean flow in a weak bubble plume for two flow rates in the laboratory and to derive a theory to interpret the underlying plume physics. Importantly, we show that weak plumes lack entrainment and grow by different physics than classic plumes. Section 2 describes the experimental set-up and the data analysis approach. In § 3, we present the direct measurement results, including the shape of the time-averaged flow velocity, the void fraction and the bubble rise velocity profiles, as well as the plume spreading. In § 4, we develop a theory to describe the mean flow parameters in the weak bubble plume, and validate the theory to the measurement data. This section provides a detailed analysis of the weak bubble plume in terms of the spreading rate of the bubble plume, the scaling of the flow velocity and the entrainment coefficient. In § 5, we present a unified scaling framework for the classic and weak bubble plumes, which also provides insight on the intermediate plume behaviour. By synthesizing the data and analyses, we show that the value of z/D determines the regime of the bubble plumes, i.e. classic plume regime with entrainment growth occurs at small z/D (e.g. previous studies where $z/D < 5$), weak plume regime with diffusive growth occurs at large z/D (e.g. the data in this study, where $z/D > 20$), and the transition occurs in the regime of $z/D \sim O(10)$. Section 6 summarizes our conclusions.

2. Methods

2.1. *Experimental set-up*

In order to study the dynamics of bubble plumes for $z/D \gg 5$, the experiments were conducted in the large-scale wave basin of the Offshore Technology Research Center (OTRC) at Texas A&M University. The wave basin is 30.5 m wide and 45.7 m long, with a primary water depth of 5.8 m. A rectangular pit (9.1 m × 4.6 m^2) is located in the centre of the basin, having a maximum water depth of 16.8 m. Air was supplied to a straight tube nozzle with an inner diameter of 0.4 mm, placed on the bottom of the pit to create a freely rising bubble plume. The confinement ratio of the plume in the pit was greater than 1×10^4, which is large enough to consider the plume as unconfined. Two designed gas flow rates, $Q_1 = 0.25$ NL min^{-1} and $Q_2 = 1.2$ NL min^{-1} at standard temperature and pressure (STP) conditions, were maintained using a fine adjustable needle valve and were measured using a mass-based gas flow meter (GFM 171, Aalborg Instruments & Controls, Inc.). The mass flow rates were also estimated from image data, which agree with the values measured with the flow meter (within 5 % difference). The length scale D for these plumes ranged from 0.02 m at the low gas flow rate to 0.08 m at the higher gas flow rate. Table 1 summarizes the experimental conditions.

Figure 1 shows a schematic of the experimental set-up and photographs of the measurement instruments. An underwater stereo imaging system (Wang & Socolofsky 2015*a*) and an acoustic Doppler velocimeter (ADV, Vectrino II profiler, Nortek), mounted on a rigid frame (see figure 1*b*), were used to measure the bubble characteristics and the centreline water velocity. The entire frame was installed at five different heights above the bottom (0.5, 3, 7, 12, and 16 m) to acquire the measured data. The frame is sufficiently large compared to the cross-sectional footprint of the bubble plumes; hence there was no obstructive effects of the frame on the dynamics of bubble plumes.

The stereo imaging system was used to quantify the bubble size, void fraction and rise velocity of the bubbles in the plume. The imaging system contains two

Parameter	Symbol	Value	Unit
Release depth	h	16.8	m
Pit dimensions	$L \times W$	9.1×4.6	m^2
Basin water density	ρ	998.3	kg m^{-3}
Gas flow rates	$\{Q_1, Q_2\}$	{0.25, 1.2}	NL min^{-1}
Nozzle diameter	d_0	0.4	mm
Released gas	—	air	—
Gas density at release	ρ_p	3.07	kg m^{-3}
Initial kinematic buoyancy fluxes	B_0	$\{1.60, 7.67\} \times 10^{-5}$	m^4 s^{-3}
Median gas bubble sizes	d_{50}	{3.8, 4.1}	mm
Gas bubble slip velocities	U_s	{0.22, 0.22}	m s^{-1}
Characteristics length scales	D	{0.017, 0.083}	m
Measurement heights	z	{0.5, 3, 7, 12, 16}	m

TABLE 1. Experimental conditions.

high-speed cameras (Vision Research Miro M340) with a 12-bit light intensity depth. These two cameras were synchronized to take images at different angles so that three-dimensional coordinates of bubbles in the scene can be determined with the precalibration of the imaging system. The bubble images were post-processed using the algorithms for bubble identification and particle tracking (Wang & Socolofsky 2015*a*). The image data were recorded in a burst mode. In each burst, cameras started with a trigger signal and stopped recording images once the internal memory of the cameras was filled. With the same internal storage (12 GB) of each camera and the same resolution of the camera (2560 pixel $\times$ 1600 pixel), the sampling rate determines the total duration of each burst. Faster sampling would yield a shorter sampling duration and *vice versa*. We have used two sample rates of 200 Hz and 24 Hz, which gave approximately 11 and 92 s burst duration. For each sample rate, three to five bursts were repeated, resulting in a total sample duration of 6 to 8 min, or approximately 17 600 to 24 000 images at each measurement height, which is adequate to obtain statistically converged results. Figure 2 shows two sample raw images from the left-hand camera at the two designed gas flow rates.

The ADV profiler was used to measure all three components of the velocity vector of the water in the centre of the bubble plume. This ADV profiler measures simultaneously the velocities of a 3.5 cm long line profile at a resolution of 0.1 cm in the radial dimension of the bubble plumes. The peak value of the measured velocities in the line profile is then taken as the centreline velocity of the plume. The noise in the ADV measurements was from two sources of error: (1) the inherent Doppler noise of the acoustic measurements, and (2) the spikes due to the interception of bubbles in the path of acoustic beams between the transmitter and the sample volume. The inherent Doppler noise only affects the Reynolds stresses and high-order velocity statistics, and the mean flow is unbiased (Voulgaris & Trowbridge 1998). Because this study focuses on the mean vertical velocity of the plumes, all the spikes have been removed in the post-processing of data. The bubble images were recorded at the same time as the ADV sampling to synchronize the measurements of the two instruments. Considering the wandering of the bubble plume, we started to record the ADV data while the centre of the plume wandered to the location of the ADV sample area and stopped sampling while the plume moved out of the sample area. Owing to the pristine water clarity in the basin, seeding particles (mean diameter of 50 μm at

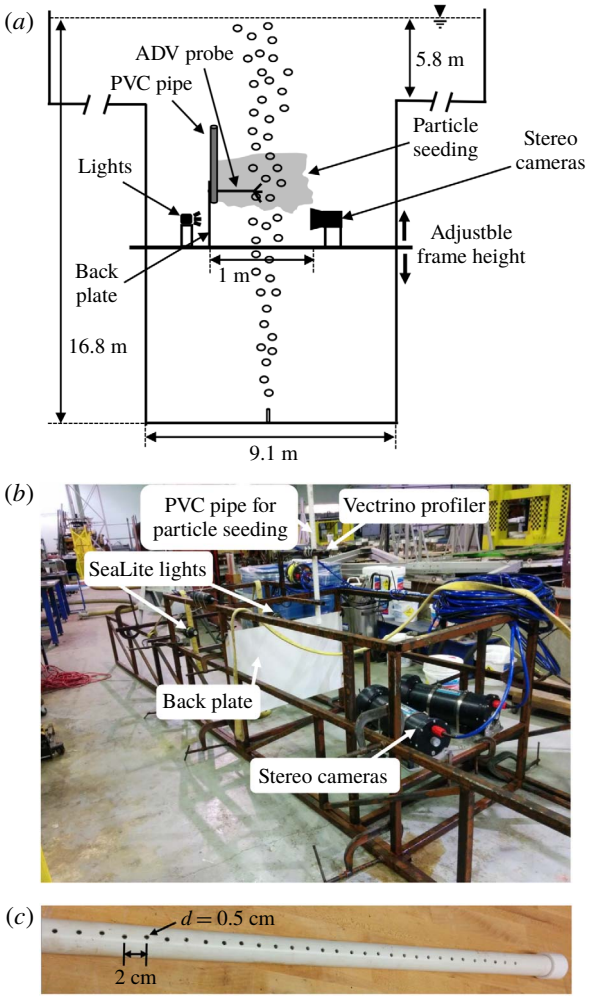

FIGURE 1. (Colour online) Presentation of experimental set-up. (*a*) Sketch of the set-up (not drawn to scale). (*b*) Photo of the frame with the installed instruments. The bubble plume is located in the centre between the cameras and the back-plate during the measurement. (*c*) The PVC pipe used for particle seeding.

approximately 1 % volume concentration) were premixed with water and seeded into the ADV sampling region during the experiment. The injection of particles created a secondary flow to the plume, as the premixed particle solution was fed using a submersible pump and was seeded horizontally from 31 holes (with 0.5 cm diameter and 2 cm spacing) in a PVC pipe (see close-up view in figure 1*c*). The distance between the seeding pipe and the centreline of the plumes was approximately 20 cm.

A test case without the bubble plume but with particle seeding was carried out to examine the velocity contribution of the seeding flow. The result shows that the mean vertical velocity generated by the seeding flow was below 0.1 cm s^{-1}, whereas the horizontal seeding speed was approximately 5 cm s^{-1}. Because the centreline water velocities due to the bubble plume measured in this study were in the range of 2 to 8 cm s^{-1}, we conclude that the mean vertical velocity due to the seeding was

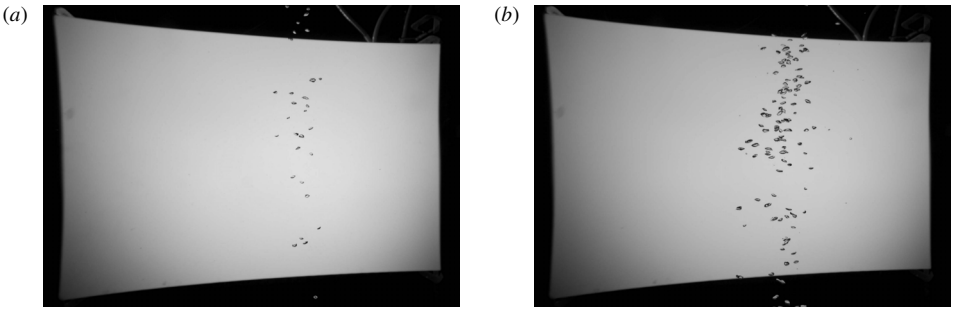

FIGURE 2. Raw sample images obtained by the stereo camera system at $z = 3$ m above the orifice; only the left camera view is shown: (*a*) $Q_1 = 0.25$ NL min^{-1}; (*b*) $Q_2 = 1.2$ NL min^{-1}.

negligible. Although the 5 cm s^{-1} horizontal speed of the seeding particles is not small, this cross-flow was only applied over a short region and only affected the flow locally. The main effect of the seeding cross-flow velocity is to displace the bubble plume centreline in the cross-flow direction at the measurement height. Because this occurred locally, the bubble plume dynamics up to the measurement point were unaffected by the seeding. We analyse the ADV strip of data to ensure that the ADV measurements always exhibit a peak velocity denoting the plume centreline within its 3.5 cm profile and confirmed from the camera images that the bubble plume centreline coincided with the ADV measurement volume. Therefore, we were able to account for the displacement caused by the seeding particles so that the induced cross-flow of the seeding was negligible on the observational results.

2.2. *Data processing*

2.2.1. *Air void fraction*

From the image data, we distinguish the gas phase from the water phase by transforming the original bubble image into a binary image, where the gas phase is denoted as 1 and the water phase is denoted as 0 (Wang & Socolofsky 2015*a*). Thus, the planar cross-sectional void fraction can be calculated

$$\chi(r) = \overline{T_g(r)/T_{total}}, \tag{2.1}$$

where $T_g(r)$ is the number of pixels occupied by the gas phase in each column of the image, and T_{total} is the total number of pixels in the vertical direction; r represents the distance to the plume centreline in the image plane. The time-averaged result is obtained by averaging over the entire image dataset at each measurement height.

2.2.2. *Time-averaged water flow velocity*

A main objective of these experiments is to quantify the continuous phase (i.e. water) mean flow characteristics of the plume caused by the rising bubbles. The procedure used to obtain the time-averaged flow velocity profile is illustrated in figure 3. The water velocities are expected to vary in the plume and to have their maximum value at the centreline of the plume. The centreline velocity was directly measured, denoted as U_{ADV} (same as the maximum profile velocity U_m in the discussion of the plume later), which is the peak value in the 3.5 cm profile of

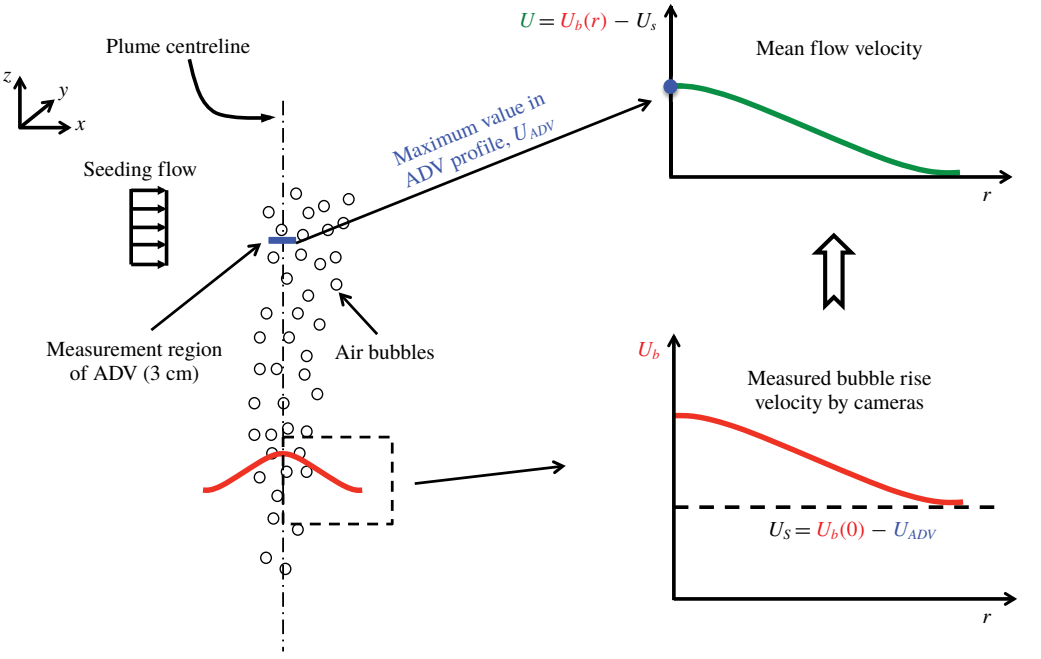

FIGURE 3. (Colour online) Sketch of time-averaged flow velocity calculation.

measured vertical velocity from the ADV. Since we measured the bubble rise velocity in the cross-section of the plume with the stereo cameras, $U_b(r)$, the cross-sectional profile of mean water velocities can be calculated from U_{ADV} and $U_b(r)$. First, we calculate the bubble slip velocity using $U_s = U_b(0) - U_{ADV}$. These slip velocities are found to be consistent with the range predicted by equations in Clift, Grace & Weber (1978) at all elevations. In our experiment, most bubbles are in the 3.5–4.5 mm range, where the bubble slip velocities are almost constant over a wide range of bubble sizes (Clift *et al.* 1978). Hence, the profile of mean water velocities can be calculated using $U(r) = U_b(r) - U_s$.

The validity of this calculation is based on the following assumptions: (1) The slip velocities of the bubbles are statistically the same across the entire cross-section. Because all bubbles have similar sizes in the cross-section, their slip velocities are expected to be similar. (2) The differences of velocity values are negligible at slightly different z for the locations of the camera and the ADV. (3) The seeding flow effect on the mean vertical velocity profile is small, which has been discussed above in § 2.1.

2.2.3. *Plume width*

A Gaussian profile has been commonly used to describe the mean flow profile of a classic bubble plume (Milgram 1983), following

$$U(r, z) = U_m(z) \exp(-r^2/b_g^2), \tag{2.2}$$

$$\chi(r, z) = \chi_m(z) \exp(-r^2/b_\chi^2), \tag{2.3}$$

where b_g and b_χ are the characteristic half-widths of the plume in terms of water velocity and void fraction. From the obtained profiles of water velocity and void fraction, the Gaussian distribution was fitted to the data, where b_g and b_χ can be determined from the fitting. The results are presented in § 3.2.

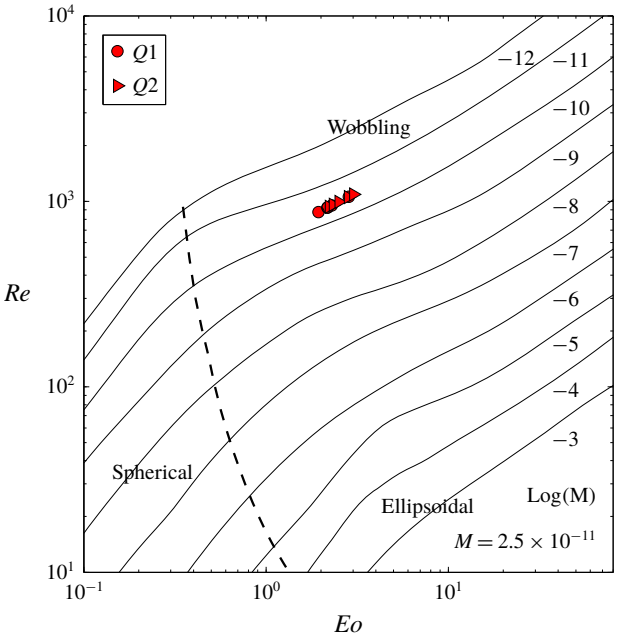

FIGURE 4. (Colour online) Shape regime of the observed bubbles. The curves are reproduced after figure 2.5 in Clift *et al.* (1978).

3. Observation results

3.1. *Bubble shape regime*

From the image data, we measured the median bubble sizes to be 3.8 and 4.1 mm for Q_1 and Q_2, respectively (see table 1). These bubbles appear to be ellipsoidal and wobbling in the video data. The quantitative presentation of bubble shape regime can be illustrated by three non-dimensional parameters: Reynolds number $Re = \rho d U_s/\mu$ (where d is bubble diameter and μ is the dynamic viscosity of water), Morton number $M = g\mu^4\Delta\rho/\overline{\rho}^2\sigma^3$ (where $\Delta\rho = (\rho - \rho_p)$ and σ is the interfacial tension), and Eötvös number $Eo = g\Delta\rho d^2/\sigma$. Values for our experiments are shown in figure 4 along with the shape regime classification in Clift *et al.* (1978). Figure 4 demonstrates that the observed bubbles are in the ellipsoidal wobbling regime of the bubble theory. Bubbles at natural seeps have also been observed to have similar shapes and sizes (Wang *et al.* 2016).

3.2. *Velocity and void fraction profiles*

In figure 5, we examine the shapes of the mean velocity and void fraction profiles in the weak bubble plume. The horizontal coordinate for the velocity and void fraction is normalized at each height by b_g and b_χ, respectively. Likewise, the velocity and void fractions are normalized by their centreline values U_m and χ_m, respectively. The irregular spacing of the velocity data is due to the fact that the velocity profile is computed from the bubbles, and the bubbles occupy discrete points and are not evenly distributed in the plume. Because the bubbles are mainly located inside the plume, the velocity data for $|r/b_g| > 1.5$ had few data points and were not statistically converged; therefore, they are not included in the figures or analysis. Despite the scatter, all data

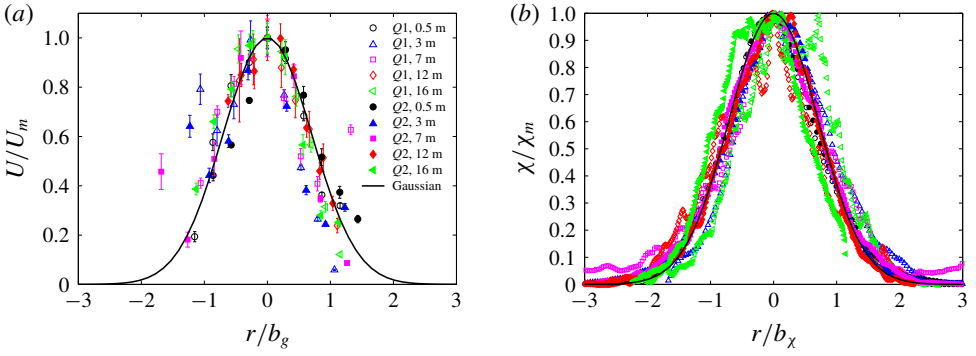

FIGURE 5. (Colour online) Self-similarity of the weak bubble plume: (*a*) mean velocity profile (error bars show standard deviation of the data); (*b*) mean void fraction profile.

appear consistent with the Gaussian distribution, with the goodness of fit $R^2 = 0.73$ and 0.95 for velocity and void fraction, respectively.

The data in figure 5 confirm the Gaussian profile shapes assumed in (2.2) and (2.3) for continuous-phase velocity and void fraction in a weak bubble plume. Although the profile shapes are preserved with height, the scales used in the non-dimensionalization (b_g, b_χ, U_m and χ_m) are not constant with height; hence, this result is not a confirmation of self-similar behaviour. Rather, these results give an analytical equation summarizing the results at each measurement height. Using the Gaussian distribution, the net upward volume flux Q in the plume is obtained as

$$Q = \int_0^\infty U(r) 2\pi r \, \mathrm{d}r = \pi b_g^2 U_m. \tag{3.1}$$

The validity of this relation is built upon the assumption of negligible gas void fraction in the plume (e.g. 0.1 % and 0.16 % in the lowest measurement location for Q_1 and Q_2, respectively). With the spreading of the bubbles in the water column, the values of void fraction decrease substantially at high locations. Equation (3.1) was used in the analysis by Leitch & Baines (1989) for a similar weak bubble plume, but they did not obtain the velocity profiles to validate the Gaussian distribution. We analyse the volume flux profile $Q(z)$ in § 4.2, where we compare entrainment models.

3.3. *Plume width and spreading rate*

The spreading rate in the lateral direction of a classic bubble plume has been shown to be similar to that for single-phase round plumes (Ditmars & Cederwall 1974), following a linear spreading behaviour given by

$$\frac{\mathrm{d}b_g}{\mathrm{d}z} = \beta, \tag{3.2}$$

where $\beta \approx 0.1$ (Fisher *et al.* 1979).

Figure 6 shows the measured relationship between the plume half-widths b_g and b_χ with the height z above the orifice in our experiments. In the linear scale plot (figure 6*a*), a reference line for linear spreading with $\beta = 0.1$ is shown as the dashed line. Comparing the measured data with the linear growth prediction, the spreading

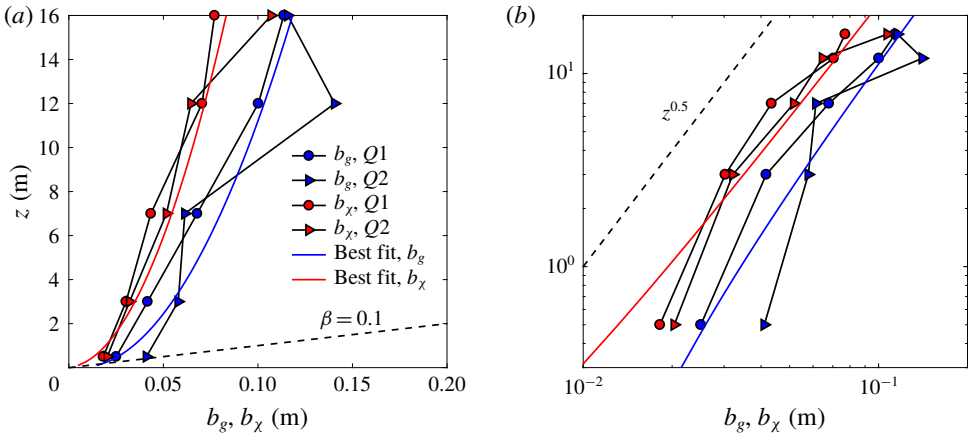

FIGURE 6. (Colour online) Half-widths of the plume at different heights above the orifice. The two solid lines without symbols represent the best fit to the data of b_χ (red line, $b_\chi = 0.021z^{1/2} - 0.002$) and b_g (blue line, $b_g = 0.028z^{1/2} + 0.006$). (*a*) Linear scale plot, where the dashed line represents the linear spreading rate in (3.2). (*b*) Log–log scale plot, where the dashed line represents the slope of a diffusive spreading process.

of the weak plume is much slower than $b_g = 0.1z$ in the current experiment. This indicates that the physical mechanism causing the spreading of the weak bubble plume differs from that for the single-phase plume and from that of the classic bubble plume. Leitch & Baines (1989) also observed a much weaker growth rate than $\beta = 0.1$ in their experiment for the cases of gas flow rate $\geqslant 0.36$ NL min^{-1}. Leitch & Baines (1989) suggested that the liquid volume flux is mostly contributed by the entrainment into the near wake of individual bubbles in the weak bubble plume, instead of the entrainment process by eddies in the turbulent shear layer of a classic bubble plume. While this may explain the flow rate, this mechanism does not directly explain the spreading rate of the plume. Also, for the lowest measurement point in our measurements ($z = 0.5$ m), the data seem to track the $b_g = 0.1z$ line, suggesting that a linear spreading region may still exist close to the bubble source. Hugi (1993) also showed a linear spreading rate of a bubble plume close to the source following $b_g = 0.1z$ that transitioned to a spreading rate that decreases further away from the source.

If we plot the plume half-width as a function of height in log–log space (figure 6*b*), the weak plume spreading follows $b_g \sim z^{1/2}$, albeit with considerable scatter of the data deviating from the best-fitting lines (especially for Q_2). The scatter of the data is almost inevitable due to the experiments being conducted at similar to field scale and due to the small values of the state variables under these weak gas flow rate conditions. The deviation of the data from the 1/2 power law growth lines could have been improved by increasing measurement locations in the experiment, which was not feasible due to our experimental constraints. The $z^{1/2}$ growth rate we argued for here has also been observed in Leitch & Baines (1989) ($b_g = 0.2z^{1/2}$), but the mechanism responsible for the 1/2 power law relationship has not been postulated. This observation suggests that the spreading of weak bubble plumes cannot be explained by the traditional bubble plume theory; hence, a new theory is needed to explain the physics of weak bubble plumes.

4. Theory of time-average dynamics of weak bubble plumes

The experimental results show that velocity and void fraction spread out with height and have a Gaussian lateral distribution, but that the spreading rates are different from the linear spreading rates for classic bubble plumes. Hence, we do not expect the integral plume equations with a constant, standard entrainment coefficient to be able to describe these results. Moreover, the much smaller spreading rates of weak bubble plumes (figure 6) suggest that a different physical process from the constant shear entrainment process in the classic plume is responsible for the weak plume dynamics. In this section, we derive a new theory to predict the bubble plume spreading and the integral plume volume flux that is applicable to weak plumes.

4.1. *Lateral spreading rates*

As shown in figure 6(*b*), the spreading of the weak bubble plume above $z = 0.5$ m height follows $b_g \sim z^{1/2}$. This region of the bubble plume behaviour is in the range of $z/D \geqslant 29$ (at low gas flow rate) and $z/D \geqslant 6.0$ (at high gas flow rate), which are both in the asymptotic regime defined by Bombardelli *et al.* (2007). In this region, the measured centreline water velocities are between 3 and 7 cm s^{-1} and the bubble rise velocities are nearly constant at 22 cm s^{-1}. This allows us to substitute time and height by $z = U_b t$, where U_b is the mean net rise velocity $U(r) + U_s$ of bubbles, taken as approximately constant. Then, we have the plume spreading as $b_g \sim t^{1/2}$, which is consistent with a diffusive process at constant diffusivity.

To model this diffusion process for plume spreading, we apply the far-field Taylor spreading theory (Taylor 1921) with an effective lateral diffusion coefficient E_t and solve for a point source:

$$\frac{\mathrm{d}b_g^2}{\mathrm{d}t} = \beta_t = 2E_t \quad \Rightarrow \quad b_g = (2E_t t)^{1/2}. \tag{4.1}$$

If we use the bubble slip velocity U_s to approximate U_b since the vertical liquid velocities are relatively small, we can convert the Lagrangian equation (4.1) to an Eulerian expression, given by

$$\frac{\mathrm{d}b_g^2}{\mathrm{d}z} = \beta_t = 2E_t U_s^{-1} \quad \Rightarrow \quad b_g = \sqrt{2}E_t^{1/2} z^{1/2} U_s^{-1/2}. \tag{4.2}$$

The measured plume width can be used with this equation to estimate E_t. We perform a regression to the measured data on the width of the plumes, which follow a linear spreading process with $b_g = 0.1z$ for $z/D < 5$ from a point source, followed by a diffusive process with $\mathrm{d}b_g^2/\mathrm{d}z = 2E_t/U_s$ for $z/D \geqslant 5$. From the regression to the data for b_g, we obtain $E_t = 8.65 \times 10^{-5}$ m^2 s^{-1} for Q_1 and 1.07×10^{-4} m^2 s^{-1} for Q_2; for fitting to data for b_χ, we obtain $E_t = 3.98 \times 10^{-5}$ m^2 s^{-1} at the lower gas flow rate and 5.02×10^{-5} m^2 s^{-1} at the higher release rate (see also table 2).

The differences in E_t estimated from b_g and b_χ relate to the different spreading rates for velocity and concentration. This effect is normally quantified by the spreading ratio λ_b, given by

$$\lambda_b = \frac{b_\chi}{b_g}. \tag{4.3}$$

Here, we can estimate λ_b by $\sqrt{E_\chi/E_g}$, as well as from the direct calculation from the definition; the values for our data are reported in table 2. These values can

Effective diffusion coefficient (unit: $\times 10^{-6}$ m^2 s^{-1})	Q_1	Q_2
E_g, E_t fitted from b_g	86.5	106.7
E_χ, E_t fitted from b_χ	39.8	50.2
$\lambda_b = \sqrt{E_\chi / E_g}$, velocity spreading ratio	0.68	0.71
$\lambda_b = b_\chi / b_g$, velocity spreading ratio	0.69	0.66
$D_{T,z}$, bubble rising direction	7.7 ± 2.2	18.5 ± 3.0
$D_{T,x}$, seeding flow direction	3.3 ± 0.3	5.8 ± 0.3
$D_{T,y}$, binormal direction	6.2 ± 2.0	13.3 ± 3.2
D_E, bubble excursion	31.0 ± 31.9	38.5 ± 37.1

TABLE 2. Effective lateral diffusion coefficient from the data fit and estimated from two different mechanisms. For D_T and D_E, mean $\pm$ standard deviation calculated from data for all heights are shown.

be compared to those reported by Socolofsky & Adams (2005), who computed λ_b between b_χ and b_c, the half-width of the concentration distribution. If we use the single-phase relationship $b_c = 1.2 b_g$, our values of λ_b reported here are similar to those in Socolofsky & Adams (2005) for bubble plumes with very weak entrained fluid velocity. Hence, the differences in the observed values of E_t for fitting to b_g and b_χ also match expectations for weak bubble plumes.

The turbulent dispersion in natural or engineered water systems can be described by an analogy to Fickian or molecular diffusion, and the diffusion coefficient is termed 'turbulent diffusivity' in turbulent flows. Since the ambient water is stagnant in the current experiment, the turbulent diffusion coefficient in the background is likely to be very low. Therefore, the diffusive process of the bubble spreading may be the result of two mechanisms: (1) the turbulent wake flow behind the leading bubbles; and (2) the lateral excursion of the bubbles, considering the zigzag or helical paths of these ellipsoidal wobbling bubbles (Wang *et al.* 2016).

Here, we estimate the effective lateral diffusion coefficient for each of the above mechanisms. First, we estimate the turbulent diffusivity (D_T) in the wake flow in three directions (i.e. bubble rising direction z, seeding flow direction x, and binormal direction y). We applied an approach derived from Taylor's theory following Holtappels & Lorke (2011), giving turbulent diffusivity $D_{Ti} = u_i' L_i = u_i'^2 T_i$, where u' is the turbulent velocity scale, L is the integral length scale, T is the integral time scale and i indicates the direction. In this work, u_i' is the standard deviation of the velocity measured by the ADV and T_i is calculated by taking the integral of the autocorrelation function of the ADV data on the centreline (Tennekes & Lumley 1972; Holtappels & Lorke 2011). The estimated turbulent diffusivity is shown in figure 7. It is seen that D_T for Q_2 is higher than that for Q_1 in all three directions, and $D_{T,z}$ is slightly larger than those in the other two directions. Overall, on the horizontal directions, D_T is in the range of 10^{-6} m^2 s^{-1}, and is approximately an order of magnitude smaller than E_t estimated from the plume spreading data.

The effective diffusion coefficient due to the second mechanism of bubble wobbling can be estimated from the product of the distance and velocity scales of the lateral excursion of the bubble motion:

$$D_E = L_E U_E, \tag{4.4}$$

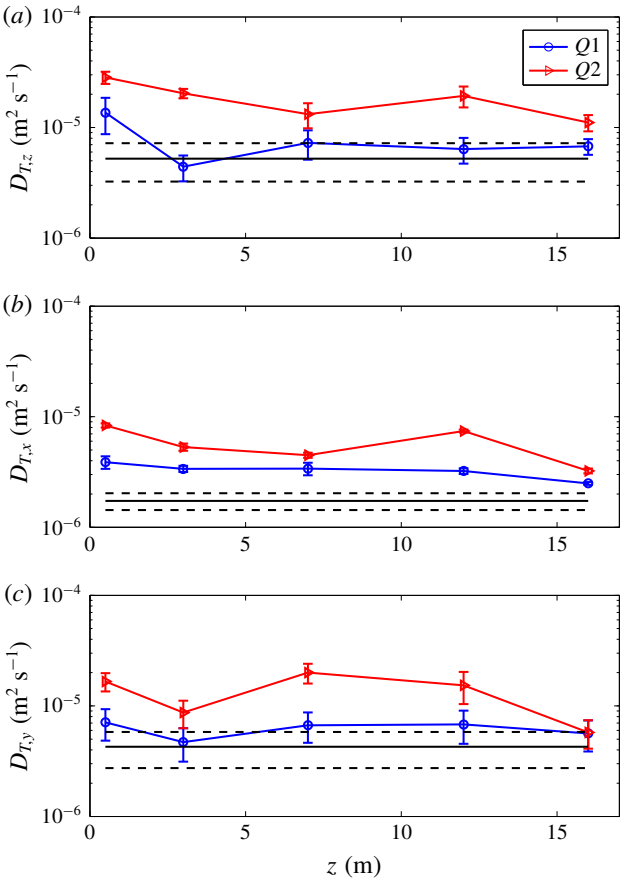

FIGURE 7. (Colour online) Turbulent diffusivity at different heights for Q_1 and Q_2, estimated using Taylor's theory (Holtappels & Lorke 2011). Symbols present the data in the bubble plumes; the solid and dashed black lines represent the mean value and standard deviation of the diffusivity in a test run without the bubble plume but with the seeding flow.

where L_E is the mean of bubble lateral excursion distance and U_E is the mean lateral velocity of the bubble excursion. The three-dimensional measurements of bubble location from the stereo camera data provide the information to compute these scales, and the calculated effective diffusion coefficients are reported in table 2. The E_t calculated by fitting the void fraction is closer to D_E than D_T. In addition, the similar E_t for both gas flow rates shown in the data may be well explained by the bubble excursion, which is determined by the bubble sizes, and is independent of the initial gas flow rate at these low flow rates. Here, we conclude that the bubble lateral excursion is probably a major contributing mechanism that is responsible for the spreading of the weak bubble plume in stagnant water, and the effective diffusion coefficient is determined by the extent and velocity of the lateral bubble motion. In more turbulent water systems, the turbulent diffusion may have a more profound contribution to the bubble plume spreading, but this is subject to further studies beyond our present scope. In any case, by these analyses, we conclude that a

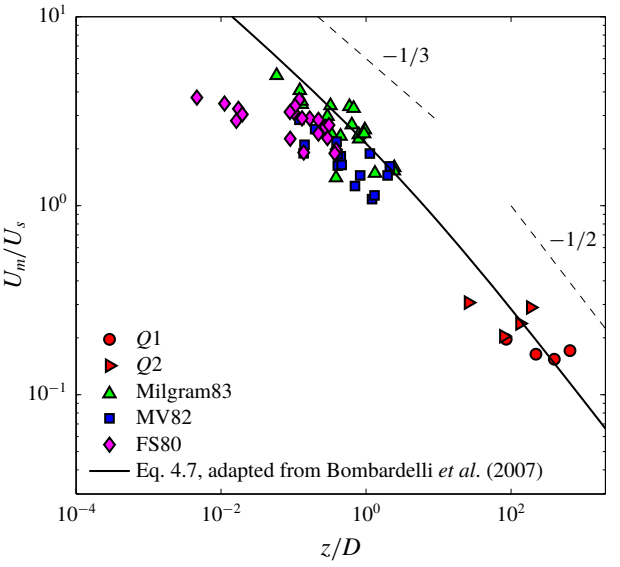

FIGURE 8. (Colour online) Normalized centreline water velocity U_m (with respect to the bubble slip velocity, U_s) versus height z above the orifice (with respect to the length scale D), where D is the length scale defined in Bombardelli *et al.* (2007). The Q_1 and Q_2 in the legend are the data of the present study. Milgram83, MV82 and FS80 represent the data summarized in Milgram (1983), including those from Fannelop & Sjoen (1980) (shown as FS80) and Milgram & Van Houten (1982) (shown as MV82). The dashed lines show the slopes of $-1/3$ and $-1/2$ for classic and weak plumes, respectively.

weak bubble plume spreads out by a diffusion process acting on the dispersed-phase particles.

4.2. *Plume centreline velocity*

The evolution of the centreline velocity with distance along the plume axis in a classic single-phase plume has been well documented. Fisher *et al.* (1979) show that the centreline velocity scales with $z^{-1/3}$ in a continuous-phase plume. For classic bubble plumes, Bombardelli *et al.* (2007) showed that

$$\frac{U_m}{U_s} \sim \left(\frac{z}{D}\right)^{-1/3}, \tag{4.5}$$

for an integral bubble plume model for $z/D < 5$. This scaling is usually assumed to be valid in a classic bubble plume (Lemckert & Imberger 1993). The data of Fannelop & Sjoen (1980), Milgram & Van Houten (1982) and Milgram (1983) are close to this scaling, although they do not collapse onto it (see figure 6a in Bombardelli *et al.* (2007) and figure 8 in the present paper).

Bombardelli *et al.* (2007) obtained an analytical solution for the centreline velocity for $z/D \gg 1$ in a classical integral bubble plume model, namely

$$\frac{U_m}{U_s} = 3\left(\frac{z}{D}\right)^{-1/2}, \quad \text{for } z/D \gg 1. \tag{4.6}$$

Bombardelli *et al.* (2007) also used numerous simulation results to obtain the asymptotic equation:

$$\frac{U_m}{U_s} = 2\left(\frac{1.9(z/D)^{-1}}{1+0.563(z/D)^{1/2}}\right)^{1/3}, \quad \text{for } z/D > 5. \tag{4.7}$$

Figure 8 shows that the non-dimensional relationship between the centreline velocity in the plume and the height above the orifice for our data ($z/D > 5$) and the literature data ($z/D < 5$) falls in the vicinity of the prediction line given by (4.7). Our data and the data from the literature span the value of z/D over four orders of magnitude. Although the discrepancy from the prediction line (4.7) grows for $z/D < 0.5$, it does pass through our weak bubble plume data and matches the observations over nearly the entire range of z/D. Thus, we will consider (4.7) valid for classic and weak bubble plumes.

This result also seems to suggest that a classic integral model can quantitatively predict the centreline velocity in both classic and weak bubble plumes. However, this asymptotic solution is solved on the basis of a linear spreading hypothesis or constant entrainment coefficient hypothesis (see also later discussion in § 4.4). As a result, it cannot predict the correct plume spreading for the weak bubble plume (see figure 6*a*), because the integral model with constant α will follow $b_g = \beta z$. Hence, the classic integral theory for a bubble plume is incapable of predicting the correct evolution of the liquid volume flux $Q = \pi b_g^2 U_m$ in weak bubble plumes ($z/D > 5$) since it will estimate a correct U_m while significantly overestimating b_g.

4.3. *Liquid volume flux*

In a general case, the relationship between Q and z in a plume is expected to follow a power law $Q \sim z^m$ (Leitch & Baines 1989). Because $\mathrm{d}Q/\mathrm{d}z \sim z^{m-1}$ represents the increase of liquid volume flux over height, which is due to the entrainment of ambient water, the value of m can be understood as follows:

(i) $m > 1$, Q increases faster than linearly (i.e. increasing entrainment);
(ii) $m = 1$, Q increases linearly (i.e. constant entrainment);
(iii) $m < 1$, Q increases slower than linearly (i.e. decreasing entrainment);
(iv) $m = 0$, Q does not change (i.e. no entrainment); and
(v) $m < 0$, Q decreases (i.e. detrainment).

From (4.5) and (3.2), the liquid volume flux in a classic integral model of a bubble plume can be derived as

$$Q = \pi b_g^2 U_m \sim \pi \beta^2 U_s D^{1/3} z^{5/3}. \tag{4.8}$$

Equation (4.8) suggests that in a classic plume Q increases faster than linearly as $m = 5/3$. Most of the literature data for bubble plumes (Fannelop & Sjoen 1980; Milgram & Van Houten 1982; Milgram 1983) have m values slightly smaller than 5/3, with the majority of these data observed in the classic bubble plume regime, below the asymptotic region (i.e. $z/D < 5$). This is a result of the presence of D, which violates the requirements for self-similarity, and expresses itself through a non-constant entrainment coefficient (or spreading rate β). Milgram (1983) developed a detailed theory for the entrainment coefficient in classic bubble plumes (see § 4.4), but most of the variability is near the source, and many successful models employ

constant entrainment coefficients (Asaeda & Imberger 1993; Bombardelli *et al.* 2007; Socolofsky, Bhaumik & Seol 2008).

Using the operational definition $Q = \pi b_g^2 U_m$, we can derive an equivalent expression in the weak bubble plume regime from our data. We select the diffusion growth process for plume spreading and substitute (4.2) for b_g. For the centreline velocity, we use the asymptotic solution at large $z/D \gg 1$ (4.6). This yields

$$Q = 6\pi E_t z^{1/2} D^{1/2}. \tag{4.9}$$

From these fitted equations, Q scales with $z^{1/2}$ in the weak plume, which demonstrates a decreasing entrainment of ambient water (i.e. $m < 1$). Therefore, the weak and classic bubble plumes have different entrainment processes (increasing and decreasing) and follow different scaling laws ($m = 1/2$ and $m = 5/3$). In the intermediate range of $z/D \sim O(1)$, m is expected to be in the range between $1/2$ and $5/3$.

Here, we also consider the similar laboratory measurements in weak bubble plumes by Leitch & Baines (1989). They observed the same bubble spreading rate ($b_g \sim z^{1/2}$) but report a different m ($m = 1$ in their work instead of $m = 1/2$ in this study). This discrepancy follows from their observation of $U_m(z) \sim z^0$ instead of $U_m(z) \sim z^{-1/2}$. Their observation may represent an accurate measurement, which the scatter in figure 8 allows, or may result from their shallow experimental water depth (i.e. 0.5 m), which may not allow adequate development of the velocity gradient to observe the $-1/2$ power law. In our experiments, the observations were conducted over 16 m of water depth, and the $-1/2$ power law is consistent across this whole water depth, linking our experiments to results reported in Milgram & Van Houten (1982). Hence, we conclude that $m = 1/2$ is the more accurate estimate of the entrainment process in a weak bubble plume.

4.4. *Apparent entrainment coefficient*

In single-phase jets and plumes, an integral model is usually closed using an entrainment hypothesis or a spreading hypothesis, and the two hypotheses are equivalent (Lee & Chu 2003) (see also appendix A). A similar spreading hypothesis was recently adapted to a particle plume (Lai *et al.* 2016). The equivalence of these two hypotheses can be summarized as follows:

$$\textit{entrainment hypothesis (for Gaussian profile)} \quad \frac{\mathrm{d}Q}{\mathrm{d}z} = 2\pi b_g \alpha U_m, \tag{4.10}$$

is equivalent to

$$\textit{jet} \begin{cases} \textit{linear spreading} & \beta_j = \dfrac{\mathrm{d}b_g}{\mathrm{d}z}, \\ \textit{dimensional analysis} & U_m = \left(\dfrac{M_0}{z^2}\right)^{1/2}, \end{cases} \tag{4.11}$$

$$\textit{plume} \begin{cases} \textit{linear spreading} & \beta_p = \dfrac{\mathrm{d}b_g}{\mathrm{d}z}, \\ \textit{dimensional analysis} & U_m = \left(\dfrac{B_0}{z}\right)^{1/3}, \end{cases} \tag{4.12}$$

where M_0 is the initial kinematic momentum flux of the jet. Thus, linear spreading of the single-phase jet and plume is mathematically equivalent to the entrainment

hypothesis with a constant entrainment coefficient α. The entrainment hypothesis states that the growth of the liquid volume flux is due to the shear entrainment of ambient liquid at the edge of the jet or plume with the entrainment velocity U_e, where U_e is proportional to the centreline velocity multiplied by the entrainment coefficient α (Turner 1986). Because the classic bubble plume spreads out linearly, similar to single-phase jets and plumes, the entrainment hypothesis in single-phase jets and plumes is adopted for many integral models of the classic bubble plume (Asaeda & Imberger 1993; Bombardelli *et al.* 2007; Socolofsky *et al.* 2008; Dissanayake, Gros & Socolofsky 2018).

For the weak bubble plume, a formulation of the integral plume equations with a constant entrainment breaks down. Instead, we derive the gradient of liquid volume flux from a spreading hypothesis, following the same procedure as in single-phase flow (see appendix A) to obtain

$$\frac{\mathrm{d}Q}{\mathrm{d}z} = \frac{1}{2}\pi\beta_b U_m, \tag{4.13}$$

with $\beta_b = \mathrm{d}b_g^2/\mathrm{d}z$. This equation differs fundamentally from the constant entrainment hypothesis (i.e. equation (4.10)). The form of (4.13) also suggests that the characteristic length scale where entrainment occurs is not b_g. We suspect that there is no entrainment at the edge of the weak bubble plume, giving $U_e = 0$. Instead, the growth of the liquid volume flux in the weak bubble plume is due to the increasing width of the plume as the result of diffusive spreading of the bubbles and the changing wake flow below the leading bubbles as they spread out. This hypothesis is also consistent with ideas in Leitch & Baines (1989), who attributed the flow rate in a weak bubble plume to the individual wakes behind bubbles.

Although we conclude for a weak bubble plume that there is no entrainment velocity in the normal sense of a plume, the equation for the growth rate of the liquid volume flux can be treated mathematically in the same manner as a classic plume, but with a different interpretation of the entrainment coefficient. If we combine (4.10) and (4.13), we can obtain the relationship

$$\alpha = \frac{\beta_b}{4b_g}. \tag{4.14}$$

Here, we name α the 'apparent entrainment coefficient', as it represents the mathematical formulation of entrainment, but in a system that does not obey the entrainment hypothesis. This equation predicts that α is not a constant and is proportional to the turbulent diffusivity causing the spread of the bubbles (β_b) and inversely proportional to the width of the plume ($b_g(z)$). Using the definitions of β_b and $b_g(z)$ in (4.2), we obtain

$$\alpha = 2^{-3/2} E_t^{1/2} U_s^{-1/2} z^{-1/2}, \tag{4.15}$$

and (4.13) becomes (this is also the direct derivative of (4.9))

$$\frac{\mathrm{d}Q}{\mathrm{d}z} = 3\pi E_t z^{-1/2} D^{1/2}. \tag{4.16}$$

Equation (4.15) predicts that the apparent entrainment coefficient α decreases with height following $\alpha \sim z^{-1/2}$ in the weak bubble plume. In a single-phase round jet or plume, the constant Gaussian entrainment coefficients are $\alpha = 0.057$ and 0.083,

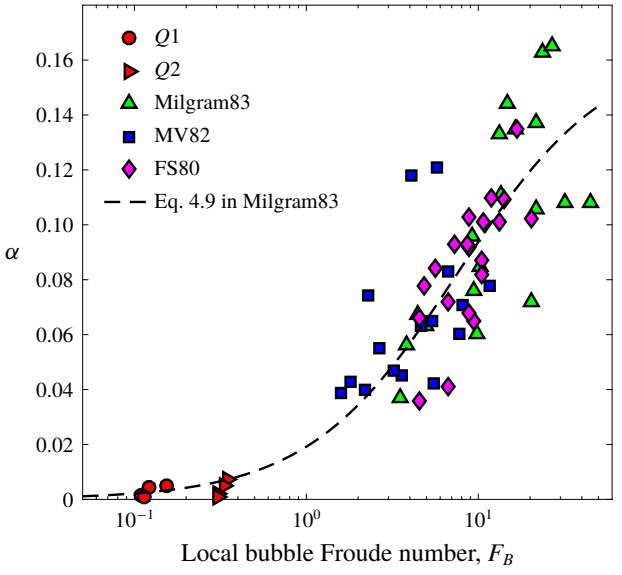

FIGURE 9. (Colour online) The relationship between α and local bubble Froude number, defined after Milgram (1983), where α is the entrainment coefficient in the classic bubble plume and is the apparent entrainment coefficient in the weak bubble plume. The dashed line represents the saturation curve proposed by Milgram (1983).

respectively (Lee & Chu 2003). Although integral models for classic bubble plumes also usually assume constant entrainment, many experimentalists have found that α is not a constant in bubble plumes, and this arises because the classic bubble plume is not strictly self-similar. Milgram (1983) used a saturation growth curve to describe the relationship between the entrainment coefficient and a local bubble Froude number (defined by $F_B = Q_b^{2/5}\chi^{1/3}g^{3/10}\Delta\rho^{1/2}\sigma^{-1/2}$, where Q_b is gas volume flux). In his empirical fit to data, the entrainment coefficient approaches a plateau at 0.16 when the local bubble Froude number increases, which occurs close to the release (e.g. $z/D \to 0$). Figure 9 compares our data with this empirical curve, where we computed the apparent entrainment coefficient α at mid-points between measurements using (4.10). The apparent entrainment coefficients in our experiment are approximately an order of magnitude smaller than entrainment coefficients reported by previous authors for larger z/D and show remarkable correspondence with the empirical fit of Milgram (1983).

Milgram (1983) interpreted the local bubble Froude number F_B as a ratio between the mixing length scale of turbulence in the plume and the characteristic length scale of bubble–bubble separation. The turbulence and the bubble–bubble separation change as the plume develops away from the source, and the resulting bubble Froude number is a complex nonlinear function of z. However, this scaling law is hidden within the z dependence of the parameters that make up F_B (e.g. χ, Q_b and $\Delta\rho$). Our analysis also predicts that $\alpha \sim z^{1/2}$ in a weak bubble plume. Hence, it is useful to evaluate the relationship between entrainment coefficient or apparent entrainment coefficient and the height above the source in the full range of the available bubble plume data. Figure 10 shows the relationship between α and z/D over a span of four orders of magnitude of z/D, including both classic and weak bubble plumes. The constant

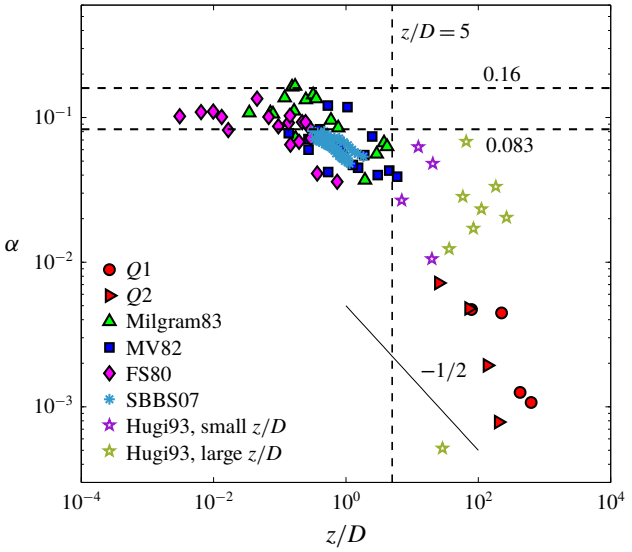

FIGURE 10. (Colour online) The relationship between α and the normalized height. The data key follows figure 8 with two additional datasets from Seol *et al.* (2007) (shown as SBBS07) and Hugi (1993) (shown as Hugi93). Hugi's data are directly digitized from the figure in Hugi (1993) and are regrouped into two regimes: (1) z/D in the same regime as our data, and (2) z/D smaller than those of our data. The solid line is the reference of $\alpha \sim z^{-1/2}$. The constant entrainment coefficient in a continuous-phase plume (i.e. 0.083) and the upper bound of a classic bubble plume (i.e. 0.16) suggested by Milgram (1983) are plotted as dashed lines.

entrainment coefficient in a continuous-phase plume, 0.083, and the plateau value in Milgram (1983), 0.16, are shown for reference. A reference line of $\alpha \sim z^{-1/2}$ is also shown, and our data agree well with this theoretical relationship in the region $z/D > 5$.

These data have had different interpretations in past papers, each supported by part of the current complete dataset of observations. An asymptotic limit of entrainment coefficient is recognized in the classic bubble plume as $z \to 0$ but the value seems not to be universal. Ditmars & Cederwall (1974) suggested 0.082 (which does appear to be the correct bound as $D \to \infty$, consistent with $U_s \to 0$) and Milgram (1983) proposed 0.16 (which here appears as a peak near $z/D \sim O(0.1)$). In addition, Seol *et al.* (2007) suggested a lower limit of entrainment coefficient (i.e. 0.04) for bubble plumes, a conclusion dominated by a single dataset of Hugi (1993). Our data show significantly smaller α compared to the cases with orders of magnitude smaller z/D in the literature and invalidate the asymptotic assumption in Seol *et al.* (2007). Our α values are also smaller than Hugi (1993) (except for one data point), although both datasets are in a similar range of z/D. The scattering of data for $z/D > 5$ might be due to the relatively large uncertainty associated with measuring $\mathrm{d}Q/\mathrm{d}z$ from a finite difference approximation using an integral quantity, an error which should be less in our deep tank (16 m) compared to Hugi (3 m). Hence, despite the scatter, the bulk of the data seem to support a decreasing trend of α versus z/D that is consistent with our scale relationship $\alpha \sim z^{-1/2}$ at large z/D.

5. Unified scaling framework for classic and weak bubble plumes

From the above analysis, it is seen that the classic and weak bubble plumes are fundamentally different. In short, the weak bubble plume does not have classic shear entrainment, but rather spreads out by diffusion of the bubbles and has increasing plume volume flux due to changes in the wakes behind individual bubbles. A hypothetical, apparent entrainment coefficient for a weak bubble plume is a function of distance along the plume z and is much smaller than for classic bubble plumes; this results in much lower spreading. Although the centreline velocity is within the prediction range of the relationship suggested by Bombardelli *et al.* (2007) (i.e. equation (4.7)), any model with a typical constant entrainment coefficient will overestimate the plume spreading, following the power law $b_g \sim z$ instead of the correct diffusive spreading rate $b_g \sim z^{1/2}$. If we simply decrease the constant entrainment coefficient in the model to match the correct apparent entrainment coefficient in the weak bubble plume, the model would fail to predict the velocity of the plume. Moreover, the linear spreading region governed by an approximately constant entrainment coefficient occurs in a narrow range of $z/D < 0.5$. Hence, no integral model with a constant entrainment coefficient can accurately predict the liquid volume flux and plume width of a weak bubble plume for $z/D \gg 1$, and it is necessary to include bubble diffusion in the plume spreading through the parameter E_t.

In this section we derive empirical scaling laws that unite the classic and weak bubble plume dynamics. For this, we classify bubble plumes into three regimes: (1) The classic bubble plume regime has a relatively stable entrainment coefficient, and the plume spreads out linearly, which is an increasing entrainment process. (2) The weak bubble regime has very small entrainment coefficient proportional to $z^{1/2}$, and the plume spreads out following a diffusive process, which is a decreasing entrainment process. (3) The intermediate bubble plume regime, between the classic and weak bubble plumes, can be considered as a transition process that smoothly connects the above two plume regimes. We separate the classic and weak bubble plumes by the region of $z/D \sim O(10)$, which is where the intermediate regime will dominate.

We compare the behaviour of the bubble plumes in the classic and weak regimes using dimensional analysis. In a bubble plume, the length scale is usually normalized with D and the velocity scale is normalized with U_s. Therefore, the non-dimensional liquid volume flux and kinematic momentum flux can be written as

$$\hat{Q} = \frac{Q}{U_s D^2}, \tag{5.1}$$

$$\hat{M} = \frac{M}{U_s^2 D^2}, \tag{5.2}$$

where $M = \pi b_g^2 U_m^2/2$. These non-dimensional equations are equivalent to $\hat{Q} \sim Q U_s^5/B_0^2$ and $\hat{M} \sim M U_s^4/B_0^2$.

In classic bubble plumes, the plume behaviour is predicted by the relationship of $\hat{Q}$ and $\hat{M}$ with the non-dimensional height above the source z/D (denoted in this section as $\hat{z}$). As shown in § 4.1, for a weak bubble plume, an additional parameter should be considered, i.e. the effective diffusion coefficient, E_t, which can be normalized as

$$\hat{E}_t = \frac{E_t}{D U_s}, \tag{5.3}$$

which is equivalent to $\hat{E}_t \sim E_t U_s^2/B_0$.

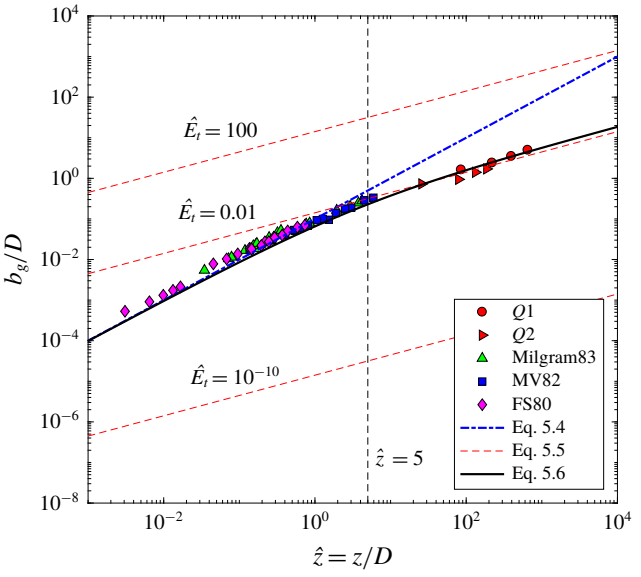

FIGURE 11. (Colour online) Non-dimensional bubble plume half-width b_g/D versus non-dimensional height z/D. We include lines for (5.4) to (5.6). See figure 8 for data key.

Using these scales, the spreading of the bubble plume can be written as

$$\textit{classic bubble plume} \quad \frac{b_g}{D} = \beta\hat{z}, \quad \text{where } \beta = 0.1, \tag{5.4}$$

$$\textit{weak bubble plume} \quad \frac{b_g}{D} = \sqrt{2}\hat{E}_t^{\,1/2}\hat{z}^{1/2}, \tag{5.5}$$

where (5.5) is derived from (4.2). To examine the behaviour of plumes in these two different regimes, figure 11 presents the measured data with reference lines for the scaling laws in (5.4) and (5.5). The data from previous authors collapse onto the (5.4) line and the data in this work collapse onto the (5.5) line with $\hat{E}_t = 0.01$. This latter curve intercepts the (5.4) line at $z/D = 5$. To obtain a universal empirical equation, we can fit an asymptotic relationship to unite the two relationships, yielding

$$\frac{b_g}{D} = \frac{0.1\hat{z}}{1 + c_1\hat{z}^{1/2}}, \tag{5.6}$$

where the coefficient $c_1 = 0.53$ is obtained by regression and having a goodness of fit $R^2 = 0.98$. This curve is also shown in figure 11.

We continue the scale analysis to predict liquid volume flux $\hat{Q}$ and momentum flux $\hat{M}$ for the classic and weak bubble plumes. For the classic bubble plume, we use the asymptotic solutions of Bombardelli *et al.* (2007) for b_g and U_m, presented previously here as (4.7) and (5.4). In the normalized format, we have

$$\hat{Q} = 2\pi\beta^2\left(\frac{1.9\hat{z}^5}{1 + 0.563\hat{z}^{1/2}}\right)^{1/3}, \tag{5.7}$$

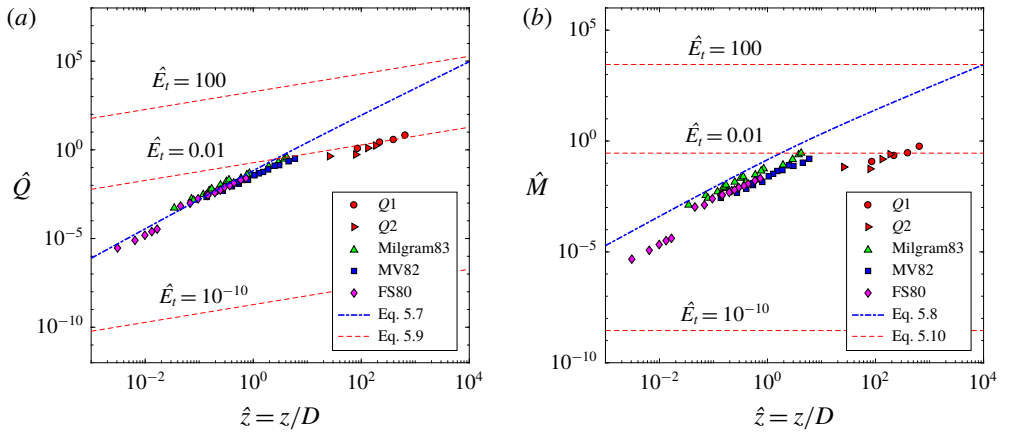

FIGURE 12. (Colour online) Non-dimensional parameters versus height in bubble plume models: (*a*) volume flux; (*b*) kinematic momentum flux. See figure 11 for data key.

$$\hat{M} = 2\pi\beta^2 \left(\frac{1.9\hat{z}^2}{1 + 0.563\hat{z}^{1/2}} \right)^{2/3}. \tag{5.8}$$

From the weak bubble plume theory, we use (4.6) and (5.5), giving

$$\hat{Q} = 6\pi\hat{E}_t\hat{z}^{1/2}, \tag{5.9}$$

$$\hat{M} = 9\pi\hat{E}_t. \tag{5.10}$$

Figure 12 shows these relationships along with the measured data.

Equations for classic and weak bubble plumes show significantly different behaviour in figure 12 (i.e. different power laws of the dash-dotted and dashed lines). Bombardelli *et al.*'s (2007) asymptotic solution tracks the volume and momentum fluxes in the classic bubble plume regime but overestimates the fluxes in the weak bubble plume regime. This is because the linear spreading theory overestimates the plume width in the weak bubble plume ($z/D \gg 1$). In contrast, the lines for the weak bubble plume at large $\hat{z}$ and with $\hat{E}_t = 0.01$ are close to our data, but the data do not exactly match the slopes of these theoretical lines, with the deviation being larger for $\hat{M}$.

In figures 11 and 12, the behaviour in the weak bubble plume regime is controlled by the effective diffusion coefficient, $\hat{E}_t$ (i.e. different dashed lines). Here we show that $\hat{E}_t = 0.01$ conforms the closest to our data for weak bubble plumes in stationary water. As discussed in § 4.1, the dimensional E_t is mainly determined by the wobbling motion of these ellipsoidal bubbles. In natural and engineered gas-in-water systems, bubbles sizes are commonly in the range of 2 to 10 mm, and these bubbles have similar bubble shape, rising trajectory and rise velocity (e.g. Clift *et al.* 1978). Therefore, we expect a small variation of E_t in any weak bubble plume, and we believe that the two flow rates in our experiments created bubbles that are representative of typical cases. Likewise, slip velocity is constant near 20 cm s^{-1} over a wide range of bubble sizes (Clift *et al.* 1978). Therefore, variation of the non-dimensional parameter $\hat{E}_t$ is probably caused by changes only in D, or correspondingly $\hat{z}$, and does not depend on the dimensional parameter E_t.

For instance, when B_0 decreases, D decreases, hence, $\hat{E}_t$ increases. Propagating this behaviour through our equations, we expect that different values of $\hat{E}_t$ will fit the data at different z/D. Hence, we might expect that, in the weak bubble plume regime, lines of constant $\hat{E}_t$ may not track the data over large regions of $\hat{z}$. This is consistent with our data's deviation from the red dashed lines in figures 11 and 12.

The data spanning over five orders of magnitude of $\hat{z}$ show that the bubble plume follows a stable entrainment process in the classic bubble plume regime, and transitions to the weak bubble plume regime occurring near the highest value of $\hat{z}$ in our dataset, where the constant entrainment coefficient is not applicable. The non-constant entrainment coefficient and different spreading processes in two regimes show significant differences from integral model predictions using constant entrainment coefficient, and these differences are dominated by bubble lateral diffusion in the weak bubble plume regime.

6. Conclusion

In this paper we presented an experimental study of a weak bubble plume in a large-scale facility at two flow rates. A theory was proposed to describe the characteristics of mean flow in the weak bubble plume and was validated with the data. We also compared the weak bubble plume closely with the classic bubble plume, to examine the similarity of the two plumes and the distinct features of the weak bubble plume. In the end, we proposed a scaling framework to unify predictions for spreading rate and volume and kinematic momentum fluxes in the classic and weak bubble plume regimes, which provides insight on the transition region between them.

The weak bubble plume has Gaussian cross-sectional profiles of velocity and cross-sectional void fraction at all heights measured above our point source diffuser. Differently from the linear spreading of the classic bubble plume, the Gaussian-defined plume radius b_g for the weak bubble plume grows following a diffusive power law $b_g \sim z^{1/2}$. The growth rate is determined by the effective diffusion coefficient E_t, which agrees with the apparent diffusion from the lateral wobbling of the rising bubbles. The contribution to this growth rate from the turbulence behind the bubble wakes is limited in stationary water. The entrainment in the weak bubble plume probably occurs in the local wake of the bubbles instead of as a shear entrainment velocity at the plume edge. The measured apparent entrainment coefficients α in the weak bubble plume are not constant and correspond well with the predictive curve proposed by Milgram (1983) as a function of local bubble Froude number. Theoretical analysis shows $\alpha \sim z^{-1/2}$ in the weak bubble plume, and this decay rate is supported by the data.

The centreline water velocities, scaled with bubble slip velocity, track the asymptotic solution proposed by Bombardelli *et al.* (2007), with $U_m \sim z^{-1/2}$ in the weak bubble plume. Taking the scaling laws for b_g and U_m together with the Gaussian profile, it follows that the liquid volume flux in the plume scales as $Q \sim z^m$ where $m = 1/2$. This predicts that the total liquid volume flux in the plume increases as the plume grows, but that the entrained liquid volume flux decreases with height. This is different from the single-phase plume and classic bubble plumes, which is an increasing entrainment process (i.e. $m = 5/3$). The available data spanning classic to weak bubble plumes are bounded by $m = 1/2$ and $5/3$.

The classic integral models for bubble plumes do not predict the behaviour of weak bubble plumes. With the traditional constant entrainment coefficient, the classic integral model predicts the correct plume velocity but overestimates the plume width

for the weak bubble plume due to its equivalent linear spreading hypothesis $b_g \sim z$. Forcing a small constant entrainment coefficient in classic integral models would fail to predict the velocity of the plume. Our analysis shows that an additional parameter, the effective diffusion coefficient E_t, is needed to correctly predict the behaviour of the weak bubble plume.

Based on the data, the theory for weak bubble plumes proposed here, and the previous theory and models for classic bubble plumes, we proposed a set of non-dimensional scaling frameworks to describe the bubble plume spreading, liquid volume flux and kinematic momentum flux for the entire regime of both classic and weak bubble plumes. We expect the scaling to give insight for bubble plumes in the transition regime between classic and weak bubble plumes. The validity of this relationship in the transition regime is subject to future studies, especially in the range of $z/D \in [10, 100]$.

Acknowledgements

This research was made possible by a grant from the Gulf of Mexico Research Initiative to the Gulf Integrated Spill Research (GISR) consortium, the Center for the Integrated Modeling and Analysis of the Gulf Ecosystem (C-IMAGE-II) consortium, and the project Synthesis of the Physical Processes in Subsea Bubble Plume to Connect Natural Seeps and Oil Spills (Syn-bubbles). Data are publicly available through the Gulf of Mexico Research Initiative Information & Data Cooperative (GRIIDC) at doi:10.7266/N7BP00T5 (Wang & Socolofsky 2016).

Appendix A

In this appendix, we derive the gradient of liquid volume flux for classic single-phase momentum jets, buoyant plumes and weak bubble plumes from a spreading hypothesis, which we then compare to the format of the equivalent entrainment hypothesis.

A.1. *Single-phase point source momentum jet*

In a self-similar pure momentum jet, the centreline velocity of the jet should be a function of z and M_0 only, where M_0 is the initial momentum flux (Fisher *et al.* 1979).

Dimensional analysis gives

$$U_m \sim \left(\frac{M_0}{z^2}\right)^{1/2}. \tag{A 1}$$

This shows that $1/U_m = \gamma z$, where γ is a constant. Taking a derivative with respect to z, we obtain

$$\frac{\mathrm{d}U_m}{\mathrm{d}z} = -\frac{U_m}{z}. \tag{A 2}$$

The linear spreading hypothesis of a momentum jet gives

$$\frac{\mathrm{d}b_g}{\mathrm{d}z} = \beta_j. \tag{A 3}$$

For a point source, $b_g = \beta_j z$. Therefore, equation (A 2) becomes

$$\frac{\mathrm{d}U_m}{\mathrm{d}z} = -\frac{U_m \beta_j}{b_g}. \tag{A 4}$$

Multiplying πb_g to both sides of this equation yields

$$\frac{\pi b_g^2}{U_m}\frac{\mathrm{d}U_m}{\mathrm{d}z} = -\pi\beta_j b_g. \tag{A 5}$$

Moving πb_g^2 inside of the derivative, with $Q = \pi b_g^2 U_m$, we have

$$\frac{\mathrm{d}Q}{\mathrm{d}z} = \pi\beta_j b_g U_m. \tag{A 6}$$

This is equivalent to the entrainment hypothesis, i.e. equation (4.10), and we have $\alpha = \beta_j/2$.

A.2. *Single-phase point source buoyant plume*

In a self-similar pure buoyant plume, the centreline velocity of the plume should be a function of z and B_0 only, where B_0 is the initial buoyancy flux.

Dimensional analysis gives

$$U_m \sim \left(\frac{B_0}{z}\right)^{1/3}. \tag{A 7}$$

This shows that $1/U_m = \gamma z^{1/3}$, where γ is a constant. Taking the z derivative, we obtain

$$\frac{\mathrm{d}U_m}{\mathrm{d}z} = -\frac{1}{3}\frac{U_m}{z}. \tag{A 8}$$

Note that this equation is in the same format as the equation for a jet (i.e. equation (A 2)).

We still have a linear spreading hypothesis in the single-phase plume. Following the same procedure for the plume from (A 3) to (A 6), we can derive the gradient of the liquid volume flux for a single-phase point source plume as

$$\frac{\mathrm{d}Q}{\mathrm{d}z} = \frac{5}{3}\pi\beta_p b_g U_m. \tag{A 9}$$

This is also equivalent to the entrainment hypothesis (4.10), and we have $\alpha = 5\beta_p/6$.

A.3. *Weak point source bubble plume*

In weak bubble plumes, the centreline velocity of the plume should be a function of z, E_t, B_0 and U_s. Bombardelli *et al.* (2007) showed (see (4.6)) that

$$U_m \sim U_s\left(\frac{z}{D}\right)^{-1/2}. \tag{A 10}$$

This shows that $1/U_m = \gamma z^{1/2}$, where γ is a constant. Taking the z derivative, we obtain

$$\frac{\mathrm{d}U_m}{\mathrm{d}z} = -\frac{1}{2}\frac{U_m}{z}. \tag{A 11}$$

This equation follows the same format as those in single-phase jets and plumes (i.e. equations (A 2) and (A 8)).

Differently from single-phase jets and plumes, the development of the weak bubble plume follows a diffusive spreading instead of linear spreading process, namely

$$\frac{\mathrm{d}b_g^2}{\mathrm{d}z} = \beta_b, \tag{A 12}$$

where $\beta_b = 2E_t/U_s$ is a constant. For a point source, we have $z = b_g^2/\beta_b$, which can be substituted in (A 11) to give

$$\frac{\mathrm{d}U_m}{\mathrm{d}z} = -\frac{1}{2}\frac{U_m\beta_b}{b_g^2}. \tag{A 13}$$

Multiplying πb_g to both sides of this equation and reorganizing gives

$$\frac{\mathrm{d}Q}{\mathrm{d}z} = \frac{1}{2}\pi\beta_b U_m. \tag{A 14}$$

This equation is not in the format of the entrainment hypothesis, as b_g is missing from the right-hand side of the equation, and β_b is of dimension $\mathcal{L}$. We discuss the physical interpretation of (A 14) in § 4.4.

REFERENCES

ASAEDA, T. & IMBERGER, J. 1993 Structure of bubble plumes in linearly stratified environments. *J. Fluid Mech.* **249**, 35–57.

BOMBARDELLI, F. A. 2004 Turbulence in multi-phase models for aeration bubble plumes. PhD thesis, University of Illinois at Urbana-Champaign.

BOMBARDELLI, F. A., BUSCAGLIA, G. C., REHMANN, C. R., RINCON, L. E. & GARCIA, M. H. 2007 Modeling and scaling of aeration bubble plumes: a two-phase flow analysis. *J. Hydraul. Res.* **45**, 617–630.

BROTHERS, L. L., VAN DOVER, C. L., GERMAN, C. R., KAISER, C. L., YOERGER, D. R., RUPPEL, C. D., LOBECKER, E., SKARKE, A. D. & WAGNER, J. K. S. 2013 Evidence for extensive methane venting on the Southeastern US Atlantic margin. *Geology* **41** (7), 807–810.

CLIFT, R., GRACE, J. R. & WEBER, M. E. 1978 *Bubbles, Drops, and Particles*. Academic Press.

CROUNSE, B. C., WANNAMAKER, E. J. & ADAMS, E. E. 2007 Integral model of a multiphase plume in quiescent stratification. *J. Hydraul. Engng ASCE* **133** (1), 70–76.

DISSANAYAKE, A. L., GROS, J. & SOCOLOFSKY, S. A. 2018 Integral models for bubble, droplet, and multiphase plume dynamics in stratification and crossflow. *Environ. Fluid Mech.* **18** (5), 1167–1202.

DITMARS, J. D. & CEDERWALL, K. 1974 Analysis of air–bubble plumes. In *Proc. Coastal Engng Conf.*, pp. 2209–2226.

FANNELOP, T. K. & SJOEN, K. 1980 Hydrodynamics of underwater blowouts. In *Proc. AIAA 18th Aerospace Sci. Meeting, Pasadena, CA*.

FISHER, H. B., LIST, E. J., KOH, R. C. Y., IMBERGER, J. & BROOKS, N. H. 1979 *Mixing in Inland and Coastal Waters*. Academic Press.

GARCIA, C. M. & GARCIA, M. H. 2006 Characterization of flow turbulence in large-scale bubble–plume experiments. *Exp. Fluids* **41** (1), 91–101.

HOLTAPPELS, M. & LORKE, A. 2011 Estimating turbulent diffusion in a benthic boundary layer. *Limnol. Oceanogr.* **9**, 29–41.

HUGI, C. 1993 Modelluntersuchungen von blasenstrahlen für die seebelüftung. PhD thesis, Inst. Hydromechanik u. Wasserwirtschaft, ETH, Zürich.

JOHANSEN, O. 2000 Deepblow – a Lagrangian plume model for deep water blowouts. *Spill Sci. Technol. Bull.* **6** (2), 103–111.

JOHNSON, H. P., MILLER, U. K., SALMI, M. S. & SOLOMON, E. A. 2015 Analysis of bubble plume distributions to evaluate methane hydrate decomposition on the continental slope. *Geochem. Geophys. Geosyst.* **16** (11), 3825–3839.

LAI, A. C. H., CHAN, S. N., LAW, A. W. K. & ADAMS, E. E. 2016 Spreading hypothesis of a particle plume. *J. Hydraul. Engng* **142**, 04016065.

LEE, J. H. W. & CHU, V. H. 2003 *Turbulent Jets and Plumes – A Lagrangian Approach*. Springer.

LEITCH, A. M. & BAINES, W. D. 1989 Liquid volume flux in a weak bubble plume. *J. Fluid Mech.* **205**, 77–98.

LEMCKERT, C. J. & IMBERGER, J. 1993 Energetic bubble plumes in arbitrary stratification. *J. Hydraul. Engng ASCE* **119**, 680–703.

MCDOUGALL, T. J. 1978 Bubble plumes in stratified environments. *J. Fluid Mech.* **85** (4), 655–672.

MCGINNIS, D. F., GREINERT, J., ARTEMOV, Y., BEAUBIEN, S. E. & WUEST, A. 2006 Fate of rising methane bubbles in stratified waters: how much methane reaches the atmosphere? *J. Geophys. Res. Oceans* **111**, C09007.

MILGRAM, J. H. 1983 Mean flow in round bubble plumes. *J. Fluid Mech.* **133**, 345–376.

MILGRAM, J. H. & VAN HOUTEN, R. J. 1982 Plumes from sub-sea well blowouts. In *Proc. of the 3rd Intl Conf. BOSS*, vol. I, pp. 659–684.

MORTON, B. R., TAYLOR, G. I. & TURNER, J. S. 1956 Turbulent gravitational convection from maintained and instantaneous sources. *Proc. R. Soc. Lond.* A **234**, 1–23.

ROMER, M., SAHLING, H., PAPE, T., BOHRMANN, G. & SPIESS, V. 2012 Quantification of gas bubble emissions from submarine hydrocarbon seeps at the Makran continental margin (offshore Pakistan). *J. Geophys. Res. Oceans* **117**, C10015.

RUPPEL, C. D. & KESSLER, J. D. 2017 The interaction of climate change and methane hydrates. *Rev. Geophys.* **55** (1), 126–168.

SCHLADOW, S. G. 1992 Bubble plume dynamics in a stratified medium and the implications for water-quality amelioration in lakes. *Water Resour. Res.* **28** (2), 313–321.

SCHLADOW, S. G. 1993 Lake destratification by bubble-plume systems – design methodology. *J. Hydraul. Engng ASCE* **119** (3), 350–368.

SEOL, D., BHAUMIK, T., BERGMANN, C. & SOCOLOFSKY, S. 2007 Particle image velocimetry measurements of the mean flow characteristics in a bubble plume. *J. Engng Mech. ASCE* **133**, 665–676.

SKARKE, A., RUPPEL, C., KODIS, M., BROTHERS, D. & LOBECKER, E. 2014 Widespread methane leakage from the sea floor on the Northern US Atlantic margin. *Nat. Geosci.* **7** (9), 657–661.

SOCOLOFSKY, S. A. & ADAMS, E. E. 2002 Multi-phase plumes in uniform and stratified crossflow. *J. Hydraul. Res.* **40**, 661–672.

SOCOLOFSKY, S. A. & ADAMS, E. E. 2003 Liquid volume fluxes in stratified multiphase plumes. *J. Hydraul. Engng ASCE* **129** (11), 905–914.

SOCOLOFSKY, S. A. & ADAMS, E. E. 2005 Role of slip velocity in the behavior of stratified multiphase plumes. *J. Hydraul. Engng ASCE* **131** (4), 273–282.

SOCOLOFSKY, S. A., BHAUMIK, T. & SEOL, D. G. 2008 Double-plume integral models for near-field mixing in multiphase plumes. *J. Hydraul. Engng ASCE* **134** (6), 772–783.

TALUKDER, A. R., ROSS, A., CROOKE, E., STALVIES, C., TREFRY, C., QI, X. B., FUENTES, D., ARMAND, S. & REVILL, A. 2013 Natural hydrocarbon seepage on the continental slope to the east of Mississippi canyon in the northern Gulf of Mexico. *Geochem. Geophys. Geosyst.* **14** (6), 1940–1956.

TAYLOR, G. I. 1921 Diffusion by continuous movements. *Proc. Lond. Math. Soc.* **20**, 196–212.

TENNEKES, H. & LUMLEY, J. L. 1972 *A First Course in Turbulence*. MIT Press.

TURNER, J. S. 1986 Turbulent entrainment – the development of the entrainment assumption, and its application to geophysical flows. *J. Fluid Mech.* **173**, 431–471.

VOULGARIS, G. & TROWBRIDGE, J. H. 1998 Evaluation of the acoustic Doppler velocimeter for turbulence measurements. *J. Atmos. Ocean. Technol.* **15**, 272–289.

WANG, B. & SOCOLOFSKY, S. A. 2015*a* A deep-sea, high-speed, stereoscopic imaging system for *in situ* measurement of natural seep bubble and droplet characteristics. *Deep Sea Res.* I **104**, 134–148.

WANG, B. & SOCOLOFSKY, S. A. 2015*b* On the bubble rise velocity of a continually released bubble chain in still water and with crossflow. *Phys. Fluids* **27**, 103301.

WANG, B. & SOCOLOFSKY, S. A. 2016 Stereoscopic camera images of low void fraction air bubble plume in stagnant water condition for experiments conducted in the Offshore Technology Research Center's 17-meter wave basin at Texas A&M University, October 2016. Distributed by: Gulf of Mexico Research Initiative Information & Data Cooperative (GRIIDC), Harte Research Institute, Texas A&M University, Corpus Christi.

WANG, B., SOCOLOFSKY, S. A., BREIER, J. A. & SEEWALD, J. S. 2016 Observation of bubbles in natural seep flares at MC 118 and GC 600 using *in situ* quantitative imaging. *J. Geophys. Res. Ocean* **121**, 2203–2230.

WEBER, T. C., MAYER, L., JERRAM, K., BEAUDOIN, J., RZHANOV, Y. & LOVALVO, D. 2014 Acoustic estimates of methane gas flux from the seabed in a 6000 km^2 region in the northern Gulf of Mexico. *Geochem. Geophys. Geosyst.* **15** (5), 1911–1925.

WESTBROOK, G. K., THATCHER, K. E., ROHLING, E. J., PIOTROWSKI, A. M., PALIKE, H., OSBORNE, A. H., NISBET, E. G., MINSHULL, T. A., LANOISELLE, M., JAMES, R. H. *et al.* 2009 Escape of methane gas from the seabed along the west Spitsbergen continental margin. *Geophys. Res. Lett.* **36**, L15608.

WUEST, A., BROOKS, N. H. & IMBODEN, D. M. 1992 Bubble plume modeling for lake restoration. *Water Resour. Res.* **28** (12), 3235–3250.

YAPA, P. D. & ZHENG, L. 1997 Simulation of oil spills from underwater accidents I. Model development. *J. Hydraul. Res.* **35** (5), 673–687.

YAPA, P. D., ZHENG, L. & NAKATA, K. 1999 Modeling underwater oil/gas jets and plumes. *J. Hydraul. Engng ASCE* **125** (5), 481–491.

ZHENG, L. & YAPA, P. D. 1998 Simulation of oil spills from underwater accidents II: Model verification. *J. Hydraul. Res.* **36** (1), 117–134.